ACS chemical biology

pubs.acs.org/acschemicalbiology

Articles

Mechanistic and Crystallographic Studies of Azoreductase AzoA from *Bacillus wakoensis* A01

Elvira Romero,[§] Simone Savino,[§] Marco W. Fraaije,* and Nikola Lončar*

Cite This: *ACS Chem. Biol.* 2020, 15, 504−512

Read Online

ACCESS | Metrics & More | Article Recommendations | Supporting Information

ABSTRACT: The azoreductase AzoA from the alkali-tolerant *Bacillus wakoensis* A01 has been studied to reveal its structural and mechanistic details. For this, a recombinant expression system was developed which yields impressive amounts of fully active enzyme. The purified holo enzyme is remarkably solvent-tolerant and thermostable with an apparent melting temperature of 71 °C. The dimeric enzyme contains FMN as a prosthetic group and is strictly NADH dependent. While AzoA shows a negligible ability to use molecular oxygen as an electron acceptor, it is efficient in reducing various azo dyes and quinones. The kinetic and catalytic mechanism has been studied in detail using steady state kinetic analyses and stopped-flow studies. The data show that AzoA performs quinone and azo dye reductions via a two-electron transfer. Moreover, quinones were shown to be much better substrates (k_{cat} values of 100−400 s^{-1} for several naphtoquinones) when compared with azo dyes. This suggests that the physiological role of AzoA and sequence-related microbial reductases is linked to quinone reductions and that they can better be annotated as quinone reductases. The structure of AzoA has been determined in complex with FMN at 1.8 Å resolution. AzoA displays unique features in the active site providing clues for explaining its catalytic and thermostability features. An uncommon loop, when compared with sequence-related reductases, forms an active site lid with Trp60 acting as an anchor. Several Trp60 mutants have been analyzed disclosing an important role of this residue in the stability of AzoA, while they retained activity. Structural details are discussed in relation to other azo and quinone reductases. This study provides new insights into the molecular functioning of AzoA and sequence-related reductases.

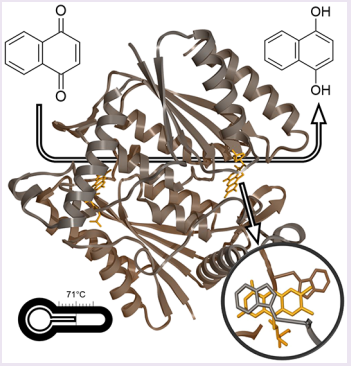

NAD(P)H-dependent flavin-containing azoreductases (EC 1.7.1.6) catalyze the reduction of azo dyes, azo pro-drugs, nitroaromatic drugs, quinones, and heavy metals.[1−6] These promiscuous biocatalysts are found in many bacteria, with close homologues in higher organisms such as yeast and mammals. Members of this diffuse redox enzyme family typically catalyze either two or four electron reductions, depending on the substrate type. For example, 2 mol of NAD(P)H are required for the reduction of 1 mol of the azo dye methyl red[7] or the nitroaromatic drug nitrofurazone.[3] When acting on quinones, azoreductases transfer only two electrons to generate the respective hydroquinones. The latter reaction is of great relevance *in vivo* to detoxify cytotoxic quinones produced as antibacterial metabolites by plants or mammals. Therefore, the participation of azoreductases in bacterial pathogenicity has been suggested.[2,8] Except for serving particular physiological roles, azoreductases are also considered for biotechnological applications. Yet, data on many of the reported azoreductases and insight into their molecular functioning is limited, and commercial availability of robust azoreductases is rather restricted.

All azoreductases exhibit a flavodoxin-like α/β-fold structure, harboring two flavin molecules at the dimer interface. Inspection of the available crystal structures has revealed that their active sites do not have enough space to simultaneously accommodate both the electron donor (NADPH and/or NADH) and acceptor.[9] Crystallographic studies of an azoreductase in complex with the NADPH analogue Cibacron Blue suggested that the NADPH C4 atom should be placed at 3.5 Å from the flavin N5 atom, allowing the hydride transfer to occur.[10] Similarly, the functional group of the electron acceptor is located above the flavin N5 atom, based on the available crystal structures.[4,10] Since the binding site of the electron donor and acceptor overlaps, a ping-pong mechanism must take place. In fact, double-reciprocal plots of initial rates of azoreductases versus the concentration of either NAD(P)H or an electron acceptor resulted in parallel lines, which is consistent with a ping-pong mechanism.[7,11]

From a biotechnological perspective, there is a great motivation for exploiting azoreductases in the detoxification of industrial effluents containing azo dyes.[12] Azo dyes are widely used in many industries such as the textiles, printing, leather, and cosmetics industries. Therefore, a more efficient, environmentally benign, and cheaper method than currently

Received: December 4, 2019
Accepted: January 22, 2020
Published: January 22, 2020

https://dx.doi.org/10.1021/acschembio.9b00970
ACS Chem. Biol. 2020, 15, 504−512

Table 1. Steady State Kinetic Parameters for WT AzoA and W60A AzoA on Four Substrates

	1,4-naphtoquinone		1,2-naphtoquinone		menadione		Orange I	
	k_{cat} (s^{-1})	K_m (μM)	k_{cat} (s^{-1})	K_m (μM)	k_{cat} (s^{-1})	K_m (μM)	k_{cat} (s^{-1})	K_m (μM)
WT	340 ± 83	97 ± 52	111 ± 7.7	61 ± 11	387 ± 60	69 ± 27	0.85 ± 0.17	115 ± 37
W60A	152 ± 34	64 ± 36	67 ± 3.4	62 ± 8	136 ± 16	25 ± 9	1.06 ± 0.14	157 ± 30

employed physical and chemical approaches for the treatment of dye-containing wastes is highly desired.[12] Azoreductases are also viewed as interesting tools for other biocatalytic processes, biosensing, and (pro)drug activation. Therefore, it is attractive to have a toolbox available of robust and tailored azoreductases with defined properties.

Azoreductases from *Bacillus cereus* and *Bacillus subtilis* were reported to be able to reduce indigo carmine, but the enzyme reaction was not studied in detail.[13,14] In 2018, another bacterial azoreductase with activity on this vat dye was reported and characterized to some extent.[15] This FMN- and NADH-dependent enzyme is intracellularly produced by *Bacillus wakoensis* AO1. This bacterial strain was isolated from an alkaline solution containing the plant *Polygonum tinctorium* used for indigo production.[15] This work prompted us to perform comprehensive biochemical, mechanistic, and crystallographic studies on this biotechnologically promising enzyme. The work presented here confirmed that AzoA is a robust NADH-dependent reductase highly active with quinones (k_{cat} values of 100−400 s^{-1}) while azo dyes are poorly accepted. An effective recombinant expression system was developed, various enzyme properties have been determined, and its crystal structure has been elucidated. The structure of this enzyme reveals unique features, different from other known azoreductases. Furthermore, the rapid kinetic studies, performed for the first time with a bacterial azoreductase, give mechanistic insights into how substrates are bound and catalysis is performed by such a reductase. The kinetic analyses strongly suggest that AzoA has a role in quinone reductions as it is highly efficient with various quinones.

RESULTS AND DISCUSSION

Production, Purification, Physicochemical Properties, and Thermostability of AzoA. While there are numerous enzymes catalyzing an impressive scope of reactions, one of the main obstacles for their detailed biochemical studies and biotechnological applications is the low production level. In the first reported study of AzoA, Suzuki *et al.* obtained a yield of 1.4 mg per liter of culture using a pET−AzoA construct.[15] With the expression constructs that we designed for this study, using pBAD-based vectors for expressing the reductase fused to His-tagged SUMO or PTDH, we reached markedly higher expression levels: 290 mg/L of SUMO−AzoA and 120 mg/L of PTDH−AzoA could be purified from 1 L of culture broth, respectively. The enzymes can be produced under standard conditions and purified using a single step of affinity chromatography purification (Figure S1). Both SUMO−AzoA and PTDH−AzoA contain noncovalently but tightly bound flavin mononucleotide (FMN) cofactor. FMN remained bound during all purification steps, including SUMO cleavage and subsequent purification. According to both gel permeation chromatography (Figure S2) and DLS experiments (Figure S3), AzoA is a dimer in solution.

By using the ThermoFAD method,[16] we assessed the stability of SUMO−AzoA in various buffers and in the presence of various cosolvents (Table S1). AzoA proved to be a very robust enzyme with apparent melting temperatures (T_m) in the range of 64−72 °C, depending on the buffer system used. This agrees with the previous observation that AzoA activity is not significantly decreased after incubating the enzyme for 1 h at 40 °C.[15] A minor positive trend in thermostability was observed when increasing the pH: the T_m increased by about 2 °C per pH unit when going from pH 8 to pH 10. This is in line with the fact that *B. wakoensis* A01 was isolated from an alkali-rich environment (Suzuki et al). AzoA also seems to tolerate cosolvents very well. Notable is the stabilizing effect of DMSO. In the presence of this cosolvent (10%, v/v), the T_m value of AzoA increased by about 5 °C (Table S1). Besides for the SUMO−AzoA, we also tested the thermostability of tag-less AzoA. This revealed that the SUMO expression tag does not influence the thermostability of AzoA. These results indicate that AzoA is a very promising enzyme for biotechnological applications.

Steady State Kinetic Analyses of Wild-Type AzoA. Some azoreductases exhibit a coenzyme preference for NADH over NADPH such as bb29AzrA-C and paAzoR2-3.[6,17] Contrarily, other azoreductases preferably use NADPH instead of NADH like paAzoR1.[6] A strict dependency for one of these electron donors has been reported for only a few azoreductases.[7−9,18,19] AzoA was reported to use only NADH as a reductant,[15] which was observed in our study as well. When we mixed SUMO−AzoA (50 nM) with NADPH (50−200 μM) in the presence of indigo carmine (50 μM), no activity could be detected. Clearly, AzoA exhibits a strict preference for NADH. When NADH was used as a coenzyme, the steady state kinetic parameters were determined for an azo dye (Orange I) and three quinones (1,4-naphthoquinone, 1,2-naphthoquinone, and menadione). This revealed that Orange I is accepted as a substrate (K_m = 115 μM and k_{cat} = 0.85 s^{-1}), but quinones seem to be much better substrates with k_{cat} values in the range of 111−387 s^{-1}, depending on the quinone (Table 1). It should be noted that in a previous study, Orange I was reported as the best azo dye substrate for AzoA, while other azo dyes (Congo red, methyl red, Orange II, and trypan blue) and alternative dyes (aniline blue and acid red 52) showed even significantly lower activities (see Figure S4).[15]

Sequence and Crystal Structure Analyses. The amino acid sequences of AzoA and thirty-three enzymes harboring flavodoxin-like structures, mostly characterized as reductases, (Table S2) were aligned by ClustalW. This revealed that AzoA presents the highest sequence identity with azoreductases from *Bacillus* sp. B29 (bb29AzrC and bb29AzrA; 55 and 43%, respectively), *B. subtilis* (bsAzoR1; 43%), and *Enterococcus faecalis* (efAzoR; 42%). A relatively high pairwise identity was also found between AzoA and bb29AzrB (37%), paAzoR3 (30%), ecAzoR (29%), paAzoR2 (25%), and paAzoR1 (23%; Table S2). Accordingly, AzoA clusters with bb29AzrC in the phylogenetic tree shown in Figure S5.

Using purified tag-less AzoA, crystals were obtained which were of a bright yellow color consistent with the flavoprotein nature of AzoA (Figure S6). The space group of the AzoA

https://dx.doi.org/10.1021/acschembio.9b00970
ACS Chem. Biol. 2020, 15, 504−512

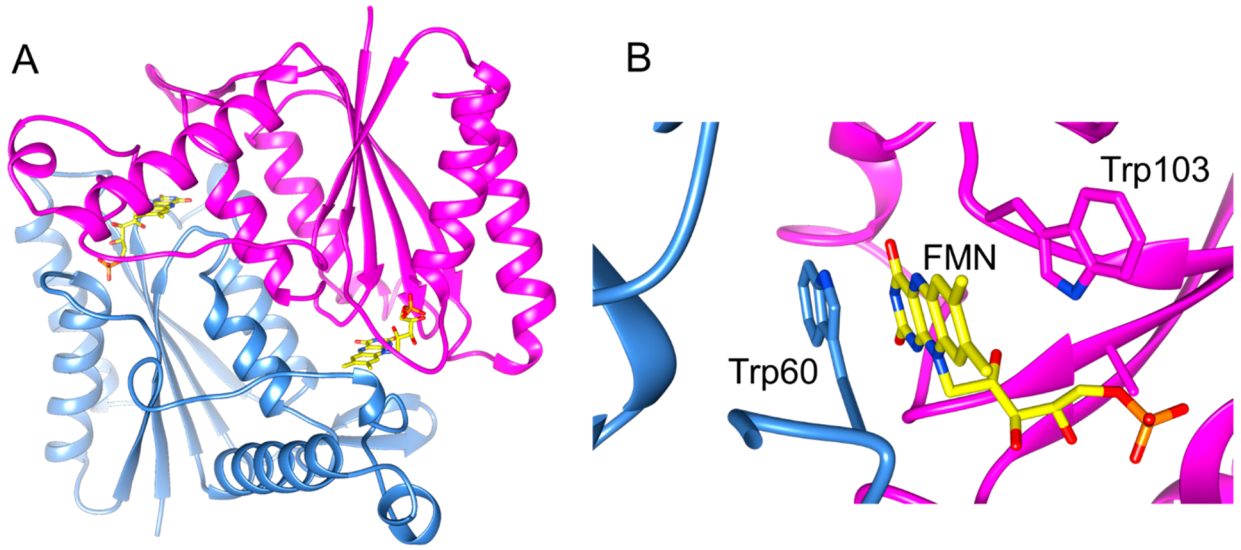

Figure 1. Crystal structure of AzoA. (A) Overall structure of the dimer, with one monomer in blue and the second in magenta; FMN is represented in yellow carbon atoms, blue nitrogen atoms, and red oxygen atoms. (B) Detail of the interface between the two monomers at the surface of the FMN binding site. Trp60 from the neighboring monomer stacks on top of the isoalloxazine of the bound FMN cofactor. PDB code: 6QU0.

crystals was found to be $P22_12_1$. The unit cell containing the protein dimer has the following dimensions a = 47.21, b = 92.97, c = 103.04, α = 90.00, β = 90.00, and γ = 90.00 (Table S3). The resolution of the elucidated protein structure is 1.8 Å, corresponding to the diffraction limit of the setup used in data collection. The Matthews coefficient[20] for the AzoA packing was calculated to be 2.40 for two molecules in the asymmetric unit, corresponding to a 48.9% solvent content, and consistent with the large channels observed in the crystal packing.

The overall structure of AzoA confirms that it forms a stable dimer (Figure 1A) similar to other azoreductases.[7,9,18,21] Numerous residues belonging to two helices (residues 104−117 and residues 159−172) are involved in the intermolecular contact between the AzoA monomers. Each monomer is structured by an alternation of alpha helices and beta sheets as previously described for structurally related reductases.[10] The tight binding of FMN is mediated by interactions with numerous residues and two water molecules (Figure S7). When compared with structures of other azoreductases, a striking structural deviation in AzoA is a relatively long loop ranging from residue 55 to residue 67. This loop contacts and closes the binding site near the FMN cofactor in the neighboring monomer. The bending of these loops into the binding pocket in front of the flavin cofactor seems to be triggered by the presence of a Trp in position 60, which interacts with the isoalloxazine ring of FMN by π-stacking (Figure 1B). This peculiar arrangement might be the result of a crystallization-induced artifact, but on the other hand, it may explain the relatively high thermostability of AzoA. The closure of the cofactor binding site by this loop, acting as a lid, prevents dissociation of the cofactor, and the increased monomer−monomer interactions may increase the structural stability of the reductase. Indeed, when Trp60 was targeted by site-directed mutagenesis, the results were in line with this hypothesis. Substituting Trp60 with Ala, Thr, Asp, Phe, or Arg causes a drastic decrease (15−25 °C) of the apparent melting temperature (Figure S8). To rationalize the relatively high thermostability of AzoA, an ensemble refinement[22] was performed on the refined structure, generating an ensemble of 50 structures based on the B factor of the atoms (Figure S9A). Globally, the AzoA structure displays only a limited flexibility, in line with its thermostability, though some flexibility is observed for the residues surrounding the binding site of FMN. The latter may reflect local protein mobility to allow substrates to dock on the protein and enter the active site. As a comparison, the same ensemble refinement was performed on the azoreductase from *Pseudomonas putida* corresponding to PDB ID 4C0W,[23] which has 31% identity with AzoA. As expected, the overall structure of 4C0W is more flexible, particularly in two loops that face the active site of the second monomer (Figure S9B). This agrees with the lack of the intersubunit stabilizing loop, containing Trp60 in AzoA. In contrast, the B factor deviation in *P. putida* azoreductase is lower for the residues surrounding the FMN binding site.

Comparison of the available crystal structures of azoreductases and other flavodoxin-like enzymes shed some light on the substrate scope of the different azoreductases. The size and hydrophobicity of the active-site pocket seem to play main roles.[10] In most flavodoxins, the isoalloxazine ring of FMN is sandwiched between two aromatic residues.[24] Generally, tryptophan and tyrosine residues flank the *re* and *si* faces of the ring, respectively. For example, *Anabaena* flavodoxin presents at these positions Trp57 and Tyr94 (PDB ID: 1FLV). These residues contribute to the stabilization of the apoflavodoxin−FMN complex, based on a comparison of binding energies of wild-type and mutant flavodoxins at the three redox states (oxidized, semiquinone, and reduced).[24] Interestingly, Tyr94 in flavodoxin favors the flavin semiquinone state relative to the hydroquinone.[24] Accordingly, the role of flavodoxins involves one-electron transfer reactions.[25] Typical azoreductases present an aromatic residue at the *re* face of the isoalloxazine ring (e.g, bb29AzrC W103, efAzoR W105, ecAzoR Y96, paAzoR1 Y98). The replacement of the corresponding Trp in efAzoR with the small residues Ala or Gly resulted in a complete loss of FMN binding affinity.[26] The result was not so dramatic when efAzoR Trp105 was replaced with Gln, Phe, or His.[26] However, azoreductases lack an aromatic residue near the *si* face of the isoalloxazine ring. Instead, the corresponding space is occupied by a ligand in many crystal structures of azoreductases. Nevertheless, their

https://dx.doi.org/10.1021/acschembio.9b00970
ACS Chem. Biol. 2020, 15, 504−512

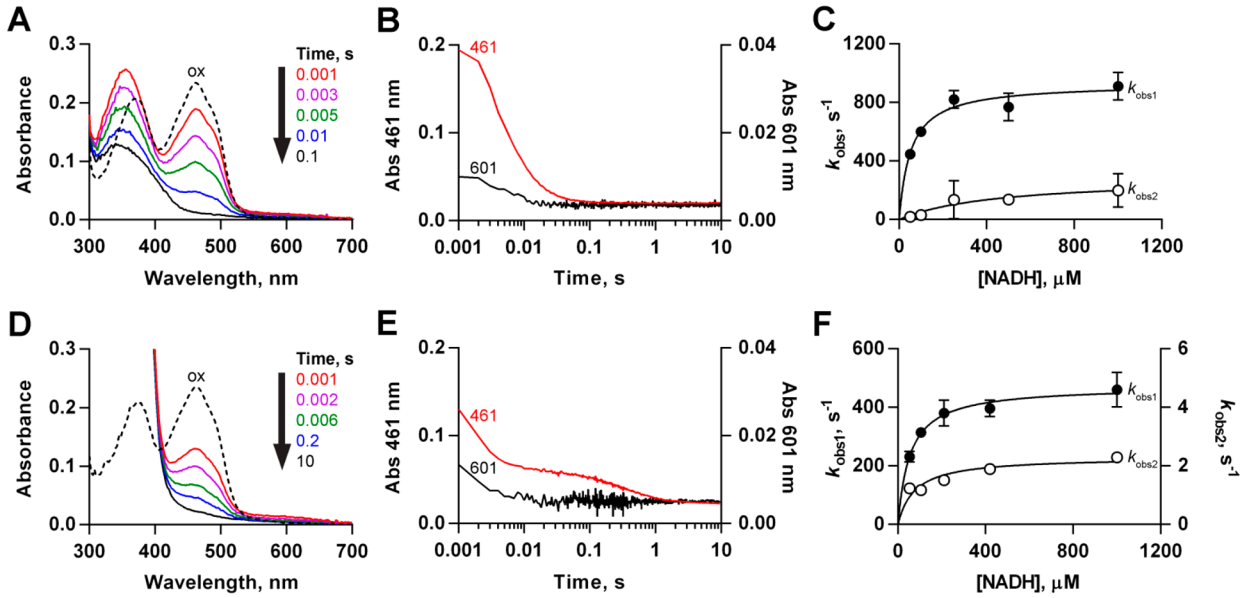

Figure 2. Anaerobic reduction of wild-type (A−C) and W60A (D−F) AzoA using NADH. (A, D) Spectral changes observed after mixing AzoA and NADH. For comparison, the spectrum of the fully oxidized enzyme is also shown (ox, broken line). Near stoichiometric amounts of wild-type enzyme and NADH were used (21 and 24 μM, respectively). In the case of W60A AzoA (21 μM), a higher amount of NADH (1000 μM) was used to observe the complete enzyme reduction in a relatively short time. A similar experiment using stoichiometric amounts of W60A AzoA and NADH is shown in Figure S12. (B, E) Selected stopped-flow traces acquired during the experiment shown in panel A and D. (C, F) Observed rates for anaerobic AzoA reduction are shown as a function of NADH concentration. To obtain these data, stopped-flow traces at 461 nm were fit with a double exponential function.

active site roof is decorated with various hydrophobic residues, which are able to interact with the aromatic substrates.[10] In the crystal structure of bb29AzrC,[10] the active site roof contains Y127, P132, and F125. These three residues are conserved in AzoA (Y127, P132, and F125). Another three residues (P11, I52, F105) were indicated to be responsible for the smaller active site of bb29AzrC, compared to that of bb29AzrA.[10] Accordingly, AzrC exhibits lower activity on large substrates than AzrA.[10] AzoA presents the same residues as bb29AzrC (P11, I52, F105). Another common residue for bb29AzrC and AzoA is the Ala at position 119, which is replaced by different residues in both bb29AzrA and bb29AzrB. A conserved Asn residue has been found forming a hydrogen bond to a hydroxyl group of the electron acceptor substrate (N104 AzrC, N99 paAzoR1, N97 ecAzoR).[10] This residue is also conserved in AzoA (N104).

When comparing the active site of AzoA, bb29AzrC, and paAzoR1, a major difference is the position and/or length of the α2 helix. This helix is closer to the substrate binding site in paAzoR1 (PDB ID: 3LT5, 3R6W, 4N65, 4N9Q) than in bb29AzrC (PDB ID: 3W78, 3W79, 3W7A). It was suggested that Phe60 paAzoR1 of the α2 helix would clash with some large substrates if they were able to bind at the active site.[10] paAzoR2 and paAzoR3 present a different residue at this position (Ser59 and Thr60, respectively), as other azoreductases, and thus its role in determining substrate specificity has been proposed.[2,4] Intriguingly, in AzoA, the α2 helix is significantly shorter and is followed by a long loop extended toward the isoalloxazine ring. The loop contains Trp60, which occupies the substrate binding site. This loop, acting as an active site lid, has not been observed in any of the available structures for azoreductases reported so far. It is evident that Trp60 must move away from the current position to allow the binding of NADH. Our mutagenesis studies on AzoA showed that Trp60 is not an essential residue for the enzyme reaction with NADH and indigo carmine. However, the mutation W60A in AzoA had a moderate influence in both enzyme reduction and reoxidation.

Steady State and Presteady State Kinetics of Wild-Type AzoA and Mutants Thereof. The particular position of Trp60 in the AzoA crystal structure prompted us to probe the function of this residue by mutating it into Ala, but also Thr, Asp, Arg, and Phe. These mutants were expressed at high levels and still displayed activity on 1,4-naphthoquinone, 1,2-naphtoquinone, menadione, and Orange I. The purified mutants also displayed flavin absorbance spectra virtually identical to wild-type AzoA (Figures S10 and S11). Steady-state kinetics data with 1,4-naphthoquinone as a substrate show that the effect of these mutations is mainly on the rate of reaction while the K_m value is only mildly influenced (Table S4). The mutation introducing a negative charge (W60D) has a more dramatic effect on the kinetic parameters, but the respective mutant enzyme still retained >10% of activity (k_{cat}).

For a more detailed analysis of the kinetic mechanism of AzoA, stopped-flow kinetic measurements were carried out. First, to study the hydride transfer reaction from NADH to AzoA, the enzyme was mixed under anaerobic conditions with the reduced coenzyme. NADH quickly converted the enzyme-bound FMN into the two-electron-reduced state, as evidenced by the decrease in the enzyme absorbance at 370 and 461 nm (Figure 2A). A significant amount of AzoA was already reduced during the dead time of the stopped-flow instrument (1 ms), even when near stoichiometric amounts of enzyme and NADH were used (21 and 24 μM, respectively, Figure 2A). Accordingly, the fully reduced enzyme was observed in less than 0.1 s at all NADH concentrations assayed (50−1000 μM NADH, 10.5 μM enzyme). The observation that the reductase was fully reduced by a near stoichiometric amount of NADH

https://dx.doi.org/10.1021/acschembio.9b00970
ACS Chem. Biol. 2020, 15, 504−512

indicates that hydride transfer in AzoA is not reversible. Stopped-flow traces at 461 nm acquired at increasing NADH concentrations were best fit with a double exponential function, with the fastest phase accounting for 93% of the total absorption change (Figure 2B). Reduction rates for both phases were dependent on NADH concentration (Figure 2C). The resulting $k_{red(NADH)}$ and $K_{d(NADH)}$ values are shown in Table 2.

Table 2. Presteady-State Kinetic Parameters of NADH-Mediated AzoA Reduction

	wild type	W60A
$k_{red(NADH)1}$ (s^{-1})	905 ± 35	472 ± 14
$k_{red(NADH)2}$ (s^{-1})	82 ± 6	2.3 ± 0.3
$K_{d(NADH)1}$ (μM)	48 ± 9	54 ± 7
$K_{d(NADH)2}$ (μM)	187 ± 38	75 ± 32
$\Delta a_1/\Delta a_2$	93/7	79/21

Only for the main reduction phase was the decrease in absorbance at 461 nm accompanied by a decrease in absorbance at 600 nm. This fact suggests the formation and decay of a charge transfer complex.[27] When the anaerobic reaction of the W60A AzoA variant with NADH was investigated under the same conditions, similar results were observed (Figure 2D–F and S12). However, the $k_{red(NADH)1}$ and $k_{red(NADH)2}$ values for the W60A AzoA variant were 2- and 36-fold lower than those for the wild-type enzyme (Table 2). Furthermore, the slowest reduction phase accounted for 21% of the total absorption change, instead of 7% observed for the wild-type AzoA. Decay of a charge transfer complex was observed for the W60A AzoA mutant as well, ruling out the possibility of a charge transfer complex involving the electron rich indole ring. Presumably, this transient charge transfer donor–acceptor interaction took place between the oxidized enzyme and NADH.[27] Altogether, these data show that AzoA is extremely efficient in using NADH as an electron donor with a flavin reduction rate of >900 s^{-1}. With such fast reduction of the flavin cofactor, the rate of catalysis will not easily be limited by the hydride transfer process. In fact, all observed k_{cat} values are well below the rate of reduction (Table 1). This contrasts with other sequence-related reductases.[28]

Reaction of Reduced AzoA with Various Electron Acceptors. The ability of reduced AzoA to use dioxygen as an electron acceptor was investigated to establish whether it can also act as an NADH oxidase. After reacting near stoichiometric amounts of AzoA and NADH (11 and 12 μM, respectively) in a vial under anaerobic conditions, the resulting reduced enzyme was mixed with various dioxygen concentrations in the stopped-flow cell. An extremely slow increase in absorbance at 461 nm was observed (0.02–0.08 s^{-1}), consistent with enzyme reoxidation (Figure 3). In all cases, it was preceded by a lag period (10–20 s), whose length decreased with the increase in dioxygen concentration. It may reflect the buildup of an initial reaction product(s), such as flavin radical species and/or superoxide, which promotes reoxidation of the reduced flavin, as observed for the reoxidation of free flavins.[29] The stopped-flow traces at 461 nm were fit with a single exponential function to determine the observed rates, which correlated linearly with the dioxygen concentration. As a result, the second-order rate constant for the reaction of the reduced enzyme with dioxygen was calculated to be 10^2 M^{-1} s^{-1}. Such low reactivity toward dioxygen clearly differentiates AzoA from oxygen-utilizing flavoenzymes. Flavoprotein oxidases and monooxygenases display rates of 10^5 to 10^6 M^{-1} s^{-1}.[30,31] Clearly, and in contrast with other azo reductases,[5] AzoA does not operate as an NADH oxidase. This prevents wasting NADH in the absence of an alternative electron acceptor and avoids formation of reactive oxygen species. While this feature is relevant for its physiological function, it also makes the enzyme an attractive biocatalyst for performing efficient quinone reductions.

The ability of various other compounds to reoxidize reduced wild-type AzoA was also investigated using the stopped-flow instrument. For these experiments, reduced AzoA (21 μM) was mixed with the same concentration of substrate under anaerobic conditions. The tested quinones (1,4-naphthoquinone, 1,2-naphthoquinone and menadione) were found to react extremely quick with reduced AzoA. Most of the reoxidation of the NADH-reduced enzyme was already achieved within the dead time of the instrument. As an example, Figure 4A shows the first spectral scan (after 2 ms) after mixing menadione with reduced AzoA, which represents nearly fully reoxidized AzoA. This confirms that quinones are exceptionally well accepted substrates reacting very fast with reduced AzoA (observed reoxidation rates of >200 s^{-1}). All tested azo compounds (Orange I, azorubine, olsalazine, and tropaeolin) resulted in very slow reoxidation of AzoA (observed rates <1 s^{-1}). As an example, Figure 4B shows the slow reoxidation of AzoA by olsalazine (an azo compound used as anti-inflammatory drug) as evidenced by the slow

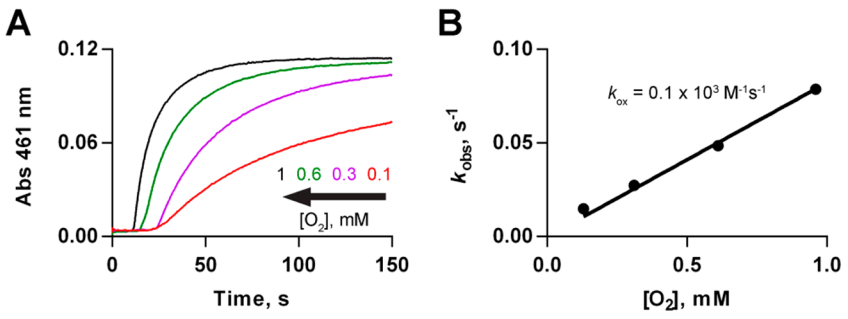

Figure 3. Reaction of anaerobically reduced wild-type AzoA with dioxygen using the stopped-flow spectrophotometer. (A) Stopped-flow traces acquired using increasing dioxygen concentrations. (B) Observed rates for AzoA reoxidation are shown as a function of dioxygen concentration. To obtain these data, stopped-flow traces at 461 nm were fit with a single exponential function. The standard error of k_{ox} was calculated to be 0.002 × 10^3.

https://dx.doi.org/10.1021/acschembio.9b00970
ACS Chem. Biol. 2020, 15, 504–512

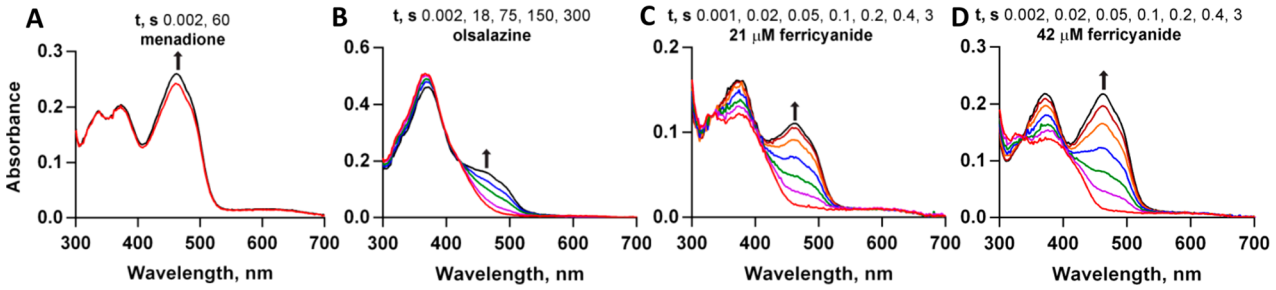

Figure 4. Reaction of anaerobically reduced wild-type AzoA with various electron acceptors using the stopped-flow spectrophotometer. Stoichiometric amounts of AzoA and NADH were mixed in a vial. The resulting reduced enzyme was mixed with the same concentration of an electron acceptor in the stopped-flow cell to observe the spectral changes (21 μM, final concentration of each reactant). All reactions took place under anaerobic conditions.

increase in absorbance at 450 nm. With all tested organic electron acceptors, the characteristic spectrum of the enzyme-bound flavin semiquinone was not observed during AzoA reoxidation (Figure 4).[28] Therefore, a direct two-electron transfer seems to take place for these reactions. Alternatively, the second electron transfer may be faster than the first one, precluding the accumulation of the radical semiquinone intermediate. The latter scenario occurred when ferricyanide was used, which is a mandatory one-electron acceptor. The evidence for this comes from the observation that the enzyme was in a 50% reduced state (no semiquinone) in the presence of a stoichiometric amount of ferricyanide (Figure 4C). Accordingly, full enzyme reoxidation was achieved with two equivalents of ferricyanide with respect to the enzyme (Figure 4D). Similarly, the characteristic spectrum of the flavin semiquinone was not observed during the reduction of DT-diaphorase with ferricyanide or the other assayed electron acceptors.[28] The ability to reduce quinones has been shown for other azoreductases such as paAzoR1-3, paArsH, paMdaB, paWrbA, and paYieF.[2,32] These enzymes reduce quinones an order of magnitude faster than they reduce azo dyes, and thus it has been suggested that quinone may be their physiological substrate.[2] There are many studies suggesting a role of azoreductases in quinone detoxification.[2,8] This is the first work on a bacterial azoreductase showing spectral evidence which supports that two electrons are transferred from the enzyme to the quinone before it is released from the enzyme active site. This reaction avoids the toxicity of quinones as oxidants and/or electrophiles.[8] The presteady state kinetic data also clearly show that AzoA is highly effective in converting quinones, while alternative electron acceptors are rather poor substrates.

The data show that wild-type AzoA is not the best candidate for bioremediation of industrial effluents containing dyes. While we observed a low activity of this enzyme on azorubine and reactive black 5, previously, it was also shown that AzoA is poorly active with Orange II, aniline blue, trypan blue, congo red, methyl red, and acid red 52.[15] It is striking to note that the enzyme is quite efficient with some specific azo dyes (Orange I and indigo carmine)[15] and quinones (menadione, 1,2-naphtoquinone, and 1,4-naphtoquinone). Except for indigo carmine, these aromatic substrates have a motif in common: a naphtoquinone moiety. It seems that there is a binding pocket in AzoA that is ideally suited for binding and reducing such naphtyl compounds. The indole moiety of indigo carmine may also be accommodated in such a pocket with its bicyclic aromatic and quinoid character.

With the structural, kinetic, and mechanistic details generated in this study, more detailed insights on how AzoA is functioning as an effective NADH-dependent quinone reductase have been obtained. Several features of this reductase are unique (well expressed, highly stability and active, no uncoupling reaction with dioxygen, active site lid), and therefore it can serve as a very suitable prototype FMN-containing reductase for future studies.

METHODS

Chemicals and Reagents. All chemicals for which the origin is not specified were purchased from Sigma-Aldrich. NADPH and NADH were purchased from Oriental Yeast Co. Ltd.

Strains, Plasmids, and Growth Conditions. The protein sequence of the azoreductase, AzoA (Genbank: BBJ25239), described by Suzuki *et al.* was used to order a synthetic gene from Integrated DNA Technologies.[15] Gene optimization was done for expression of AzoA in *Escherichia coli*, and the sequence of the synthetic gene is given in the SI of this manuscript and has been submitted to GenBank (MK674977). Using Golden Gate assembly, the gene was cloned into a pBAD vector generating two constructs for expressing AzoA with an N-terminal fusion partner: (a) AzoA fused with His-tagged SUMO (His6-SUMO), resulting in SUMO−AzoA, and (b) AzoA fused to His-tagged phosphite dehydrogenase (His6-PTDH), resulting in PTDH−AzoA. Primers and plasmid maps are available upon request. Plasmid sequences were verified by sequencing (Eurofins Genomics). Recombinant SUMO−AzoA and PTDH−AzoA were overexpressed and purified according to the following procedure: *E. coli* NEB10β cells were freshly transformed with the corresponding plasmid, and an overnight culture was diluted 50-fold into 400 mL of Terrific Broth medium with 50 μg/mL ampicillin (TB_{amp}) in 2 L baffled flasks. Cells were induced at OD_{600} = 1.5 with 0.02% w/v L-arabinose (final concentration) and incubated at 25 °C for 40 h (135 rpm). Cells were harvested at 4 °C and centrifuged at 4000*g* for 20 min. They were resuspended in 50 mM TRIS/HCl buffer pH 8.0 containing 0.5 M NaCl and 0.1 mM phenylmethylsulfonyl fluoride (PMSF), disrupted by sonication in an ice/water bath and centrifuged at 4 °C 19800*g* for 60 min. The cell-free extract was applied in a 5 mL Ni-Sepharose FF gravity column pre-equilibrated in 50 mM TRIS/HCl buffer at pH 8.0 with 0.5 M NaCl. Stepwise elution was used to wash nonspecifically bound proteins, and elution of SUMO−AzoA and PTDH−AzoA was achieved with 50 mM TRIS/HCl at pH 8.0, 0.5 M NaCl, and 500 mM imidazole. Purified SUMO−AzoA (in further text referred to as AzoA) and PTDH−AzoA were desalted into 50 mM TRIS/HCl at pH 8.0 using EconoPac desalting columns (Bio Rad) and flash frozen in liquid nitrogen. Samples were stored at −70 °C until further use. The concentration of purified FMN-containing AzoA was determined based on the wild-type enzyme extinction coefficient at 461 nm (11.1 mM^{-1} cm^{-1}), which was determined as previously described using trichloroacetic acid as a denaturing agent.[33]

Proteolytic digestion of the SUMO-tag was done to prepare an AzoA sample for crystallization. SUMO−AzoA (2 mL, 10 mg mL^{-1})

https://dx.doi.org/10.1021/acschembio.9b00970
ACS Chem. Biol. 2020, 15, 504−512

was incubated with SUMO protease (1 mg mL^{-1}) overnight at 4 °C on a nutating shaker and then for 3 h at RT. The reaction mixture was applied on a pre-equilibrated Ni-Sepharose column, and the flow-through fraction, containing cleaved AzoA, was collected. Non-digested SUMO−AzoA, cleaved SUMO-tag, and SUMO-protease were then eluted with 50 mM TRIS/HCl at pH 8.0 containing 0.5 M NaCl and 500 mM imidazole. All fractions were analyzed using SDS-PAGE (12% gel).

Thermostability Assays. The ThermoFAD method[16] was used to determine the apparent melting temperature of SUMO−AzoA at different pH values or in the presence of different additives. Using an RT-PCR machine (CFX96-Touch, Bio-Rad), the fluorescence of the flavin cofactor was monitored using a 450−490 excitation filter and a 515−530 nm emission filter, typically used for SYBR Green based RT-PCR. The temperature was increased 0.5 °C per step, starting at 25 °C and ending at 90 °C, using a holding time of 10 s at each step. The maximum of the first derivative of the observed flavin fluorescence was taken as the apparent melting temperature. Twenty microliters of the enzyme solution containing 10 μM SUMO−AzoA and the additive (solvent or buffer of appropriate pH) was put into a 96-well PCR plate and covered with a transparent adhesive film; then the ThermoFAD assay was run.

Determination of Oligomerization State. After digestion with SUMO protease and removal of protease and His6-SUMO tag, the purified AzoA samples were concentrated to 10 mg mL^{-1}. A 500 μL sample was injected into a Superdex75 10/300 column (GE Healthcare) connected to an Äkta purifier (GE Healthcare). A calibration curve was made using a commercial gel permeation standard (Bio Rad).

Dynamic lights scattering (DLS) measurements were performed in a 5 μL disposable cuvette using a DynaPro NanoStar instrument (Wyatt Technology). The DLS results were analyzed with dynamics software, version 7 (Wyatt Technology).

Steady State Kinetic Analysis. Kinetic assays were performed in duplicate for 60 s using a Jasco V-660 spectrophotometer. Different concentrations of substrates (0.01−0.5 mM) were dissolved in 50 mM TRIS/HCl at pH 8.5. The final concentration of methanol in the reactions was kept below 1% (v/v). AzoA (final concentration 0.01−0.05 μM) was added to the reaction mixture, and the reaction was started by the addition of 0.15 mM NADH (final concentration). NADH consumption (ε_{340} = 6220 M^{-1} cm^{-1}) was followed at 340 nm in the case of quinones, while reduction of indigo carmine was followed at 610 nm using ε_{610} = 19 400 M^{-1} cm^{-1}[34] and reduction of α-naphthol orange (Orange I) was followed at 500 nm using ε_{500} = 20 900 M^{-1} cm^{-1}. All data were analyzed using the software GraphPad Prism 6.05 (La Jolla, CA, USA).

Rapid Kinetics Analysis. The catalytic and kinetic mechanism of AzoA was investigated using a SX20 stopped-flow spectrophotometer in single-mixing mode (Applied Photophysics). Absorbance spectra and single wavelength traces were acquired with a photodiode array and photomultiplier detection, respectively. The software Pro-Data 4.2.12.0 (Applied Photophysics) or GraphPad Prism 6.05 was used to analyze all data. Assays were run in duplicate or triplicate by mixing equal volumes of two reactants, at 25 °C. All solutions were prepared in 50 mM TRIS/HCl at pH 8.5. For anaerobic experiments, 100% nitrogen was bubbled through the substrate solutions (2.0 mL) containing 5.0 mM glucose. Next, 5.0 μL of glucose oxidase (*Aspergillus niger*, type VII, Sigma-Aldrich) was added (0.30 μM, final concentration) to remove traces of residual dioxygen. The enzyme was made anaerobic by the same procedure, except that nitrogen was blown on the surface of the solution. The flow circuit of the stopped-flow instrument was deoxygenated by repeated washes with nitrogen-bubbled buffer containing 5.0 mM glucose and 0.30 μM glucose oxidase.

To study AzoA reduction using NADH as an electron donor, the enzyme (10.5 μM) was mixed with various NADH concentrations (50−1000 μM) in the stopped-flow cell under anaerobic conditions. Absorbance traces at 461 nm were recorded and fit to an appropriate exponential function to determine the observed rates (k_{obs}). A plot of the k_{obs} values versus NADH concentrations was fit to a rectangular hyperbola to calculate the pseudo-first-order rate constant for anaerobic enzyme-bound FMN reduction under saturation conditions (k_{red}) and the apparent macroscopic dissociation constant for binding of the substrate to the enzyme (K_d). Similarly, near stoichiometric amounts of enzyme and NADH were mixed (21 and 24 μM, respectively) in the stopped-flow cell to record consecutive absorbance spectra (300−700 nm) during the reaction.

The reoxidation of anaerobically reduced AzoA was studied using the following potential electron acceptors: dioxygen, indigo carmine, azorubine, reactive black 5, menadione, 1,2-naphthoquinone, ferricyanide, olsalazine, and tropaeolin. First, reduced enzyme was prepared in a vial under anaerobic conditions (2.0 mL), by adding a small aliquot (<10 μL) of NADH. Stoichiometric or near stoichiometric concentrations of the reactants were used, as indicated for each experiment. The resulting solution was mixed in the stopped-flow cell with an electron acceptor to observe the resulting spectral changes. When dioxygen was used as electron acceptor, the desired final dioxygen concentrations (0.13, 0.31, 0.61, and 0.96 mM) were achieved as previously described.[35] For all experiments, the stopped-flow traces at an appropriate wavelength were fit to an exponential function to determine the k_{obs} values. The second-order rate constant for the reaction of dioxygen was calculated from the slope of the linear plot of k_{obs} as a function of dioxygen concentration.

Crystallization and X-ray Analysis. A concentrated sample of AzoA (24 mg mL^{-1}), prepared by digestion with SUMO protease and gel permeation (*vide supra*), was used for crystallization experiments. Different sparse matrix screens from Molecular Dimensions (JCSG+, LMB, BCS, PACT) were tested by dispensing the conditions and the protein sample using a Mosquito robot (TTP Labtech) in 96-well two-drop Swissci plates for sitting drop (Molecular Dimensions). Drops were set at 5:3 and 3:5 ratios of a protein and reservoir mix. The protein solution was supplemented with 1.0 mM FMN and 1.0 mM NAD^+. Multiple positive hits were found after 1−2 days of storage at 20 °C, and they were reproduced by setting handmade crystallization experiments using the same protein concentration and a 1:1 ratio for protein/reservoir. Crystals were reproduced in VDX plates for hanging drop crystallization (Hampton research). The most reproducible condition was found to be the D9 of the JCSG+ screen, containing 0.17 M ammonium sulfate and 25.2% (w/v) PEG 4000 (Figure S6). Plates were prepared ranging in concentrations of 0.1−0.2 M ammonium sulfate and 20−30% (w/v) PEG 4000.

AzoA crystals, grown in the conditions described above, were harvested and shortly passed in a cryoprotectant solution identical to the reservoir mix and supplemented with 20% glycerol. The harvested crystals were directly mounted on the goniometer of the in-house diffractometer (MarDTB Goniostat system) for preliminary characterization and data collection. Images were collected with the detector distance set at 140 mm, corresponding to a maximal theoretical resolution of 1.79 Å for our in-house setup. For one crystal, 600 images were collected at a ΔΦ of 0.3 per image, for a total of 180°. The collected images were indexed and integrated in *iMosflm* and the so generated *.mtz* file used to run *aimless* from the CCP4 suite for scaling.[36] The scaled *.mtz* file was used in *phaser*[37] together with the *.pdb* 3W7A[10] as a search model for structure solution (55% identity). The structure of 3W7A was previously prepared by running *chainsaw*[38] to keep only the side chains of conserved residues. The model was refined by running *refmac5*,[36] alternated to manual fitting in *coot*.[39]

Site-Directed Mutagenesis. The Agilent primer design tool (www.agilent.com) was used to design the primers to create mutants W60A, W60T, W60D, W60F, and W60R using QuikChange site-directed mutagenesis. Oligonucleotide sequences are available upon request. Two primers were used in each PCR reaction, using the *Pfu*Ultra II Master Mix (Agilent) as recommended by the supplier. The pBad-SUMO−AzoA construct was used as a template which results in expression of AzoA mutants with a N-terminal 6xHis-SUMO tag. Mutants were expressed and purified as described above for the wild-type enzyme.

Phylogenetic Analysis. A phylogenetic tree of AzoA and other enzymes harboring the flavodoxin-like structure was constructed using

https://dx.doi.org/10.1021/acschembio.9b00970
ACS Chem. Biol. 2020, 15, 504−512

the Neighbor-joining method. A bootstrap consensus tree was prepared, which was inferred from 500 replicates. Table S2 shows the GenBank codes for the 34 amino acid sequences selected for these analyses. The alignment required for the phylogenetic tree was generated by ClustalW. All analyses were performed using the MEGA7 software.[40]

■ ASSOCIATED CONTENT

Supporting Information

The Supporting Information is available free of charge at https://pubs.acs.org/doi/10.1021/acschembio.9b00970.

AzoA sequences, Supporting Figures 1−12, and Supporting Tables 1−4 (PDF)

■ AUTHOR INFORMATION

Corresponding Authors

Marco W. Fraaije − *Molecular Enzymology Group, University of Groningen, 9747AG Groningen, The Netherlands;* orcid.org/0000-0001-6346-5014; Email: m.w.fraaije@rug.nl

Nikola Lončar − *GECCO Biotech, 9747AG Groningen, The Netherlands; Molecular Enzymology Group, University of Groningen, 9747AG Groningen, The Netherlands;* Email: n.loncar@gecco-biotech.com

Authors

Elvira Romero − *Molecular Enzymology Group, University of Groningen, 9747AG Groningen, The Netherlands*

Simone Savino − *Molecular Enzymology Group, University of Groningen, 9747AG Groningen, The Netherlands*

Complete contact information is available at: https://pubs.acs.org/10.1021/acschembio.9b00970

Author Contributions

[§]Contributed equally

Notes

The authors declare the following competing financial interest(s): E.R. is currently a Postdoctoral Researcher at AstraZeneca R&D Gothenburg.

■ ABBREVIATIONS

T_m, melting temperature; NAD^+, nicotinamide adenine dinucleotide; SUMO, small ubiquitin-like modifier; PTDH, phosphite dehydrogenase; FMN, flavin mononucleotide

■ REFERENCES

(1) Ackerley, D. F., Gonzalez, C. F., Park, C. H., Blake, R., Keyhan, M., and Matin, A. (2004) Chromate-reducing properties of soluble flavoproteins from *Pseudomonas putida* and *Escherichia coli*. *Appl. Environ. Microbiol. 70*, 873−882.

(2) Crescente, V., Holland, S. M., Kashyap, S., Polycarpou, E., Sim, E., and Ryan, A. (2016) Identification of novel members of the bacterial azoreductase family in *Pseudomonas aeruginosa*. *Biochem. J. 473*, 549−558.

(3) Ryan, A., Kaplan, E., Laurieri, N., Lowe, E., and Sim, E. (2011) Activation of nitrofurazone by azoreductases: Multiple activities in one enzyme. *Sci. Rep. 1*, 63.

(4) Ryan, A., Laurieri, N., Westwood, I., Wang, C. J., Lowe, E., and Sim, E. (2010) A novel mechanism for azoreduction. *J. Mol. Biol. 400*, 24−37.

(5) Suzuki, H. (2019) Remarkable diversification of bacterial azoreductases: Primary sequences, structures, substrates, physiological roles, and biotechnological applications. *Appl. Microbiol. Biotechnol. 103*, 3965−3978.

(6) Ryan, A., Wang, C. J., Laurieri, N., Westwood, I., and Sim, E. (2010) Reaction mechanism or azoreductases suggests convergent evolution with quinone oxidoreductases. *Protein Cell 1*, 780−790.

(7) Nakanishi, M., Yatome, C., Ishida, N., and Kitade, Y. (2001) Putative ACP phosphodiesterase gene (acpD) encodes an azoreductase. *J. Biol. Chem. 276*, 46394−46399.

(8) Leelakriangsak, M., Huyen, N., Töwe, S., Van Duy, N., Becher, D., Hecker, M., Antelmann, H., and Zuber, P. (2008) Regulation of quinone detoxification by the thiol stress sensing DUF24/MarR-like repressor, YodB in *Bacillus subtilis*. *Mol. Microbiol. 67*, 1108−1124.

(9) Ito, K., Nakanishi, M., Lee, W. C., Sasaki, H., Zenno, S., Saigo, K., Kitade, Y., and Tanokura, M. (2006) Three-dimensional structure of AzoR from *Escherichia coli*. An oxidereductase conserved in microorganisms. *J. Biol. Chem. 281*, 20567−20576.

(10) Yu, J., Ogata, D., Gai, Z., Taguchi, S., Tanaka, I., Ooi, T., and Yao, M. (2014) Structures of AzrA and of AzrC complexed with substrate or inhibitor: Insight into substrate specificity and catalytic mechanism. *Acta Crystallogr., Sect. D: Biol. Crystallogr. 70*, 553−564.

(11) Wang, C. J., Laurieri, N., Abuhammad, A., Lowe, E., Westwood, I., Ryan, A., and Sim, E. (2010) Role of tyrosine 131 in the active site of paAzoR1, an azoreductase with specificity for the inflammatory bowel disease prodrug balsalazide. *Acta Crystallogr., Sect. F: Struct. Biol. Cryst. Commun. 66*, 2−7.

(12) Chengalroyen, M. D., and Dabbs, E. R. (2013) The microbial degradation of azo dyes: Minireview. *World J. Microbiol. Biotechnol. 29*, 389−399.

(13) Božič, M., Kokol, V., and Guebitz, G. M. (2009) Indigo dyeing of polyamide using enzymes for dye reduction. *Text. Res. J. 79*, 895−907.

(14) Pricelius, S., Held, C., Murkovic, M., Bozic, M., Kokol, V., Cavaco-Paulo, A., and Gübitz, G. M. (2007) Enzymatic reduction of azo and indigoid compounds. *Appl. Microbiol. Biotechnol. 77*, 321−327.

(15) Suzuki, H., Abe, T., Doi, K., and Ohshima, T. (2018) Azoreductase from alkaliphilic *Bacillus* sp. AO1 catalyzes indigo reduction. *Appl. Microbiol. Biotechnol. 102*, 9171−9181.

(16) Forneris, F., Orru, R., Bonivento, D., Chiarelli, L. R., and Mattevi, A. (2009) ThermoFAD, a thermofluor-adapted flavin ad hoc detection system for protein folding and ligand binding. *FEBS J. 276*, 2833−2840.

(17) Ooi, T., Shibata, T., Matsumoto, K. I., Kinoshita, S., and Taguchi, S. (2009) Comparative enzymatic analysis of azoreductases from *Bacillus* sp. B29. *Biosci., Biotechnol., Biochem. 73*, 1209−1211.

(18) Chen, H., Wang, R., and Cerniglia, C. E. (2004) Molecular cloning, overexpression, purification, and characterization of an aerobic FMN-dependent azoreductase from *Enterococcus faecalis*. *Protein Expression Purif. 34*, 302−310.

(19) Leelakriangsak, M., and Borisut, S. (2012) Characterization of the decolorizing activity of azo dyes by *Bacillus subtilis* azoreductase AzoR1. *Songklanakarin J. Sci. Technol. 34*, 509−516.

(20) Kantardjieff, K. A., and Rupp, B. (2003) Matthews coefficient probabilities: Improved estimates for unit cell contents of proteins, DNA, and protein-nucleic acid complex crystals. *Protein Sci. 12*, 1865−1871.

(21) Ooi, T., Shibata, T., Sato, R., Ohno, H., Kinoshita, S., Thuoc, T. L., and Taguchi, S. (2007) An azoreductase, aerobic NADH-dependent flavoprotein discovered from *Bacillus* sp.: Functional expression and enzymatic characterization. *Appl. Microbiol. Biotechnol. 75*, 377−386.

(22) Forneris, F., Burnley, B. T., and Gros, P. (2014) Ensemble refinement shows conformational flexibility in crystal structures of human complement factor D. *Acta Crystallogr., Sect. D: Biol. Crystallogr. 70*, 733−743.

(23) Goncalves, A. M., Mendes, S., de Sanctis, D., Martins, L. O., and Bento, I. (2013) The crystal structure of *Pseudomonas putida* azoreductase - the active site revisited. *FEBS J. 280*, 6643−6657.

(24) Lostao, A., Gómez-Moreno, C., Mayhew, S. G., and Sancho, J. (1997) Differential stabilization of the three FMN redox forms by

tyrosine 94 and tryptophan 57 in flavodoxin from *Anabaena* and its influence on the redox potentials. *Biochemistry 36*, 14334−14344.
(25) Nogués, I., Pérez-Dorado, I., Frago, S., Bittel, C., Mayhew, S. G., Gómez-Moreno, C., Hermoso, J. A., Medina, M., Cortez, N., and Carrillo, N. (2005) The ferredoxin-NADP(H) reductase from *Rhodobacter capsulatus*: Molecular structure and catalytic mechanism. *Biochemistry 44*, 11730−11740.
(26) Chen, H., Xu, H., Kweon, O., Chen, S., and Cerniglia, C. E. (2008) Functional role of trp-105 of *Enterococcus faecalis* azoreductase (AzoA) as resolved by structural and mutational analysis. *Microbiology 154*, 2659−2667.
(27) Massey, V., and Ghisla, S. (1974) Role of charge-transfer interactions in flavoprotein catalysis. *Ann. N. Y. Acad. Sci. 227*, 446−465.
(28) Tedeschi, G., Chen, S., and Massey, V. (1995) DT-diaphorase: Redox potential, steady-state, and rapid reaction studies. *J. Biol. Chem. 270*, 1198−1204.
(29) Gibson, Q. H., and Hastings, J. W. (1962) The oxidation of reduced flavin mononucleotide by molecular oxygen. *Biochem. J. 83*, 368−377.
(30) Chaiyen, P., Fraaije, M. W., and Mattevi, A. (2012) The enigmatic reaction of flavins with oxygen. *Trends Biochem. Sci. 37*, 373−380.
(31) Gadda, G. (2012) Oxygen activation in flavoprotein oxidases: The importance of being positive. *Biochemistry 51*, 2662−2669.
(32) Ryan, A., Kaplan, E., Nebel, J. C., Polycarpou, E., Crescente, V., Lowe, E., Preston, G. M., and Sim, E. (2014) Identification of NAD(P)H quinone oxidoreductase activity in azoreductases from *P. aeruginosa*: Azoreductases and NAD(P)H quinone oxidoreductases belong to the same FMN-dependent superfamily of enzymes. *PLoS One 9*, No. e98551.
(33) Macheroux, P. (1999) UV-visible Spectroscopy as a Tool to Study Flavoproteins, in *Flavoprotein Protocols*, (Chapman, S. K., and Reid, G. A., Eds.) pp 1−7, Humana Press, New Jersey.
(34) Sousa, M. M., Miguel, C., Rodrigues, I., Parola, A. J., Pina, F., Seixas de Melo, J. S., and Melo, M. J. (2008) A photochemical study on the blue dye indigo: From solution to ancient andean textiles. *Photochem. Photobiol. Sci. 7*, 1353−1359.
(35) Lončar, N., Fiorentini, F., Bailleul, G., Savino, S., Romero, E., Mattevi, A., and Fraaije, M. W. (2019) Characterization of a thermostable flavin-containing monooxygenase from *Nitrincola lacisaponensis* (NiFMO). *Appl. Microbiol. Biotechnol. 103*, 1755−1764.
(36) Winn, M. D., Ballard, C. C., Cowtan, K. D., Dodson, E. J., Emsley, P., Evans, P. R., Keegan, R. M., Krissinel, E. B., Leslie, A. G., McCoy, A., McNicholas, S. J., Murshudov, G. N., Pannu, N. S., Potterton, E. A., Powell, H. R., Read, R. J., Vagin, A., and Wilson, K. S. (2011) Overview of the CCP4 suite and current developments. *Acta Crystallogr., Sect. D: Biol. Crystallogr. 67*, 235−242.
(37) McCoy, A. J., Grosse-Kunstleve, R. W., Adams, P. D., Winn, M. D., Storoni, L. C., and Read, R. J. (2007) Phaser crystallographic software. *J. Appl. Crystallogr. 40*, 658−674.
(38) Stein, N. (2008) CHAINSAW: A program for mutating pdb files used as templates in molecular replacement. *J. Appl. Crystallogr. 41*, 641−643.
(39) Emsley, P., and Cowtan, K. (2004) Coot: Model-building tools for molecular graphics. *Acta Crystallogr., Sect. D: Biol. Crystallogr. 60*, 2126−2132.
(40) Kumar, S., Stecher, G., and Tamura, K. (2016) MEGA7: Molecular evolutionary genetics analysis version 7.0 for bigger datasets. *Mol. Biol. Evol. 33*, 1870−1874.

https://dx.doi.org/10.1021/acschembio.9b00970
ACS Chem. Biol. 2020, 15, 504−512